Image blur in high energy proton radiography *

WEI Tao(魏涛)[1)] YANG Guo-Jun(杨国君) LONG Ji-Dong(龙继东) SHI Jin-Shui(石金水)

Institute of Fluid Physics, China Academy of Engineering Physics, P.O. Box 919-106, Mianyang 621900, China

Abstract: Proton radiography has provided a potential development direction for advanced hydrotesting, and its image blur is a crucial point that needs to be deeply studied. In this article, numerical simulation by using the Monte Carlo code Geant4 has been implemented to investigate the entire physics mechanism of high energy proton beam travelling through the object and beamline and arriving at the image plane. This article will mainly discuss the various factors which cause the image blur, including the chromatic aberration of the imaging beamline, the insufficient modulation of an incident particle's transverse displacement and angle deviation, the longitudinal length of an object, the influence of containment vessel and otherwise.

Key words: proton radiography, image blur, chromatic aberration, scattering, containment vessel

PACS: 29.27.Eg **DOI:** 10.1088/1674-1137/37/6/068201

1 Introduction

The proton radiography [1–3] (pRad) technique is a new and much more capable diagnostic tool for hydrotest experiments. In comparison with classical flash X-rays radiography [4], pRad has higher penetrating power, higher detection efficiency, less scattered background, inherent multi-pulse capability, more exact material identification and a large standoff distance between the objects and detectors [5].

Early in the 1960s, A. M. Koehler pointed out that pRad could be used to make unusually high contrast radiographs [6, 7] of an object. It is a pity that such a technique was abandoned because of poor position resolution [6] and multiple Coulomb scattering (MCS) leading to the image blur in pRad which is about an order of magnitude larger than that in flash X-rays radiographs [8].

Till now, pRad depending on the use of a particular magnetic lens to compensate for MCS has been developed [1], and pRad has been demonstrated to provide data on dynamic systems, which is far superior to that which can be obtained with flash X-rays.

2 The pRad lens system

Because the incident proton particles undergo MCS in the object, a special magnetic lens system is needed to focus the particles from the object point to the image point. The beam optics requirements for a pRad lens system are well understood and schematically shown in Fig. 1. The different colors represent the different scattering angles within the object.

There are two primary requirements of the pRad lens system [9]. First, the lens system must provide a point-to-point focus from object to image. Second, it must form a Fourier plane, where particles can be sorted by the scattering angle. With the latter requirement, particles with large scattering angles can be removed through transverse collimation at the Fourier plane. To satisfy the above demands, the incident particle's transverse displacement x and angle deviation along beam direction x' must be strongly correlated,

$$x'/x=\omega, \tag{1}$$

in which ω is the correlation coefficient, the angle sorting function can be carried out.

3 The image blur

An additional requirement, which is usually a strong design driver for a pRad lens, is the resolution of the radiography system [1]. To improve the resolution, the image blur should be as small as possible.

3.1 The chromatic aberration blur

The pRad image blur is typically dominated by chromatic aberrations due to energy spread in the incident beam in combination with the spread of energy loss

Received 16 July 2012

∗ Supported by National Natural Science Foundation of China (11205144), National Natural Science Foundation of China (11176001) and Science and Technology Development Program of China Academy of Engineering Physics (2010A042016)

1) E-mail: weitaocaep@sohu.com

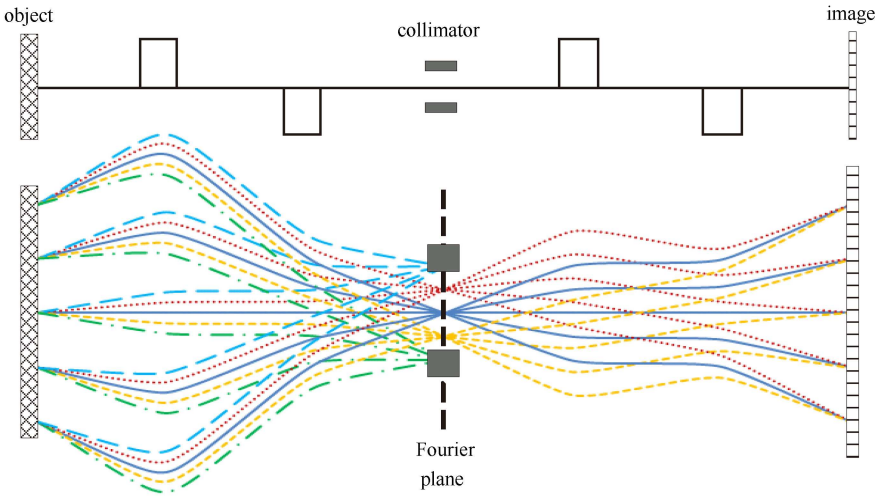

Fig. 1. Schematic diagram of a pRad lens system showing the point-to-point focus of particle trajectories (colored lines) from object to image.

through the object. The chromatic aberration blur can be expressed as [7, 10, 11]

$$\Delta x_{\rm ch}=T_{116}x\delta+T_{126}x'\delta+T_{126}\theta\delta, \tag{2}$$

in which θ is the deviation angle due to MCS and $\delta=\Delta p/p_0$ is the relative momentum deviation, p_0 is the momentum of reference particle, T_{116} and T_{126} represents the second order chromatic aberrations in TRANSPORT notation. For the pRad lens system, the second terms should satisfy the equation [11] as follows,

$$T_{116}+\omega T_{126}=0. \tag{3}$$

Combining Eqs. (1)–(3), the chromatic aberration blur [11] is

$$\Delta x_{\rm ch}=T_{126}\theta\delta. \tag{4}$$

To acquire perfect performance, the chromatic aberration blur should be small enough. Both θ and δ scale inversely with the beam momentum, so better resolution is expected with higher beam momentum. The chromatic coefficients, T_{126} (for x direction) and T_{346} (for y direction), are decided by the lens system. To decrease the chromatic coefficients, the feasible scheme is to increase the field gradients of the magnet lens and then shorten the longitudinal distance of the pRad lens system [12].

The scattering angle θ is caused mainly by MCS. When a proton beam passes through an object, the proton particles undergo lots of MCS which is well described by a Gaussian distribution at the exit of the object, and the root mean square (RMS) plane projection scattering angle [13] θ_0 is

$$\theta_0=\frac{13.6\ {\rm MeV}}{p\beta c}\sqrt{z}[1+0.038\ln(z)], \tag{5}$$

where c is the velocity of light, βc is the velocity of the proton, p is its momentum, $z=L/L_{\rm R}$ is the object length measured in units of radiation length, L is the length of the object and $L_{\rm R}$ is the radiation length.

In this article, numerical simulation using the Monte Carlo code Geant4 [14] has been implemented to investigate the entire physics mechanism. In simulation, some self-field effects were ignored, for example the space charge effect and wake field effect. The particle number was 2×10^5, which was tested to be convergent. And the occupied time is about 5 hours each time by using a personal computer.

What is shown in Fig. 2 is the simulation results by GEANT4. When the 50 GeV proton beam passes through the object perpendicularly, the scattering angle distribution approximates a Gaussian type. To ignore the blur caused by the object length, the object length was set as to be small as possible in simulation code and

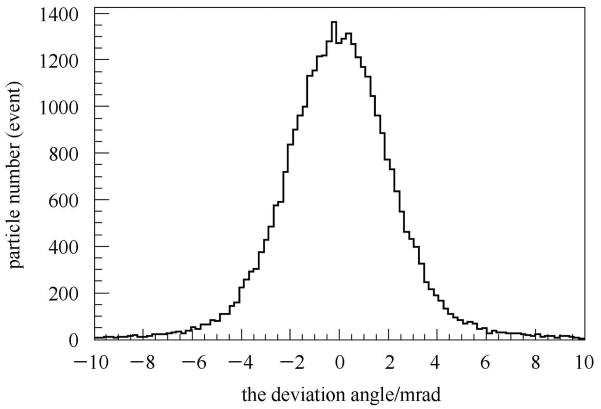

Fig. 2. The scattering angle distribution of 50 GeV proton beam passing through the uranium object simulated by Geant4. The areal density is 200 g/cm^2.

the mass density was set large enough to keep the areal density invariable. We chose a long uranium object of 200 g/cm^2 and a radiation length of 0.32 cm, the RMS plane projection deflection angle was 2.35 mrad, which is in good agreement with Formula (5).

The momentum deviation is caused mainly by ionization reaction. As shown in Fig. 3(a), when the reference particle's momentum is the same as that of the incident particles, i.e., 50929.63 MeV/c, the distribution of momentum deviation is nearly a Landau type [13]. After Monte Carlo simulation, the distribution of momentum deviation and the chromatic aberration blur are shown in Fig. 3. The RMS chromatic aberration blur is 0.45 mm.

Furthermore, we can choose the energy of reference particle by changing the magnetic field grads of the quadrupole magnets. For example, when the momentum of the reference particle is appointed as 50669.63 MeV/c, the RMS chromatic aberration blur is 0.08 mm. The distribution of momentum deviation and the chromatic aberration blur are shown in Fig. 4. It is clear that the chromatic aberration blur decreases evidently.

3.2 The blur caused by object length

The MCS will result in the deviation of the particle's trace from a straight line in the object, and it has two effects. The first one is the chromatic aberration blur previously mentioned, which will result in a transverse position offset between the image and the object's counterpoint in the image plane because the chromatic coefficients T_{126} and T_{346} are non-zero. The second one is the random walk itself, which will result in the change of the particle's transverse displacement in the object plane, and then the blur occurs because the object point changes. The latter blur is correlative with the length of object, so we call it blur caused by the object length. As shown in Fig. 5, the incident particle undergoes lots of Coulomb scatterings, and travels out of the object with deviation distance x_z. As can be seen in Fig. 5, the object plane locates at the center plane of the object, then the object point is the intersection of the ejaculate particle and the object plane. So the deviation distance x_m equals the blur caused by the object length, i.e., $\Delta x_{\rm ol}=x_m$.

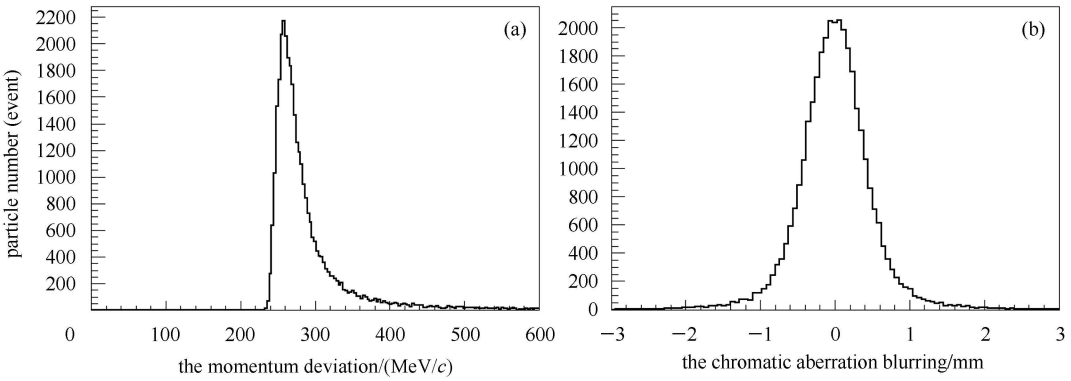

Fig. 3. The distribution of momentum deviation (a) and the chromatic aberration blur (b) simulated by Geant4 when the 50 GeV proton beam passes through the 200 g/cm^2 long uranium object.

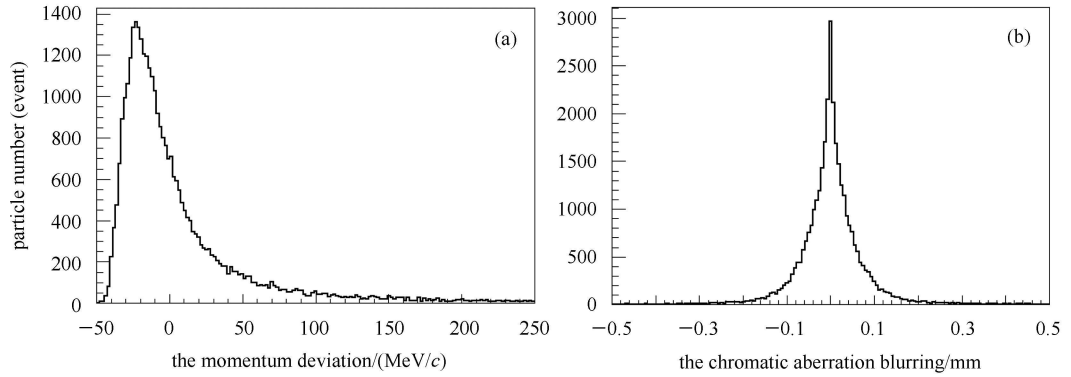

Fig. 4. The distribution of momentum deviation (a) and the chromatic aberration blur (b) simulated by Geant4 after changing the magnetic field grads of quadrupole lens.

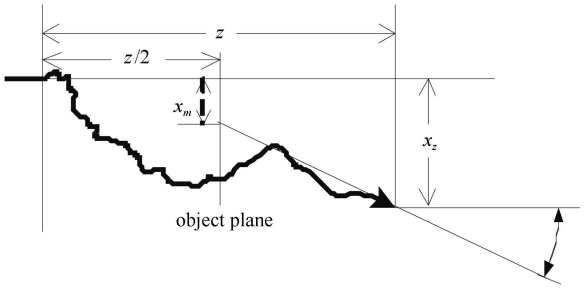

Fig. 5. The sketch map of an incident particle passing through the object.

The probability where the incident particle is found within $\mathrm{d}z\mathrm{d}x_z\mathrm{d}\theta$ district in the object can be expressed as [6]

$$F(z,x_z,\theta)=\frac{\sqrt{3}}{2\pi}\frac{w^2}{z^2}\exp\left[-w^2\left(\frac{\theta^2}{z}-\frac{3x_z\theta}{z^2}+\frac{3x_z^2}{z^3}\right)\right], \quad (6)$$

in which $w=2p\beta c/E_s$ and

$$E_s=m_\mathrm{e}c^2\left(\frac{8\pi^2\mathrm{e}^2}{hc}\right)^{1/2}=21.205\ \mathrm{MeV}.$$

The conditional probability that the particle is located at certain z and θ is given by

$$\begin{aligned} G(z,\theta) &= \int_{-\infty}^{+\infty}F(z,x_z,\theta)\mathrm{d}x_z \\ &= \frac{1}{2\sqrt{\pi}}\frac{w}{z^{1/2}}\exp\left[-\frac{1}{4}(w^2\theta^2/z)\right], \end{aligned} \quad (7)$$

and the RMS deflection angle is given by

$$\theta_\mathrm{rms}=\sigma_\theta=\sqrt{\frac{2z}{w^2}}=\frac{15.0\ \mathrm{MeV}}{p\beta c}\sqrt{z}. \quad (8)$$

Of course the RMS deflection angle should be revised as Formula (5).

The conditional probability that the particle is located at certain z and x_z is given by

$$H(z,x_z)=\int_{-\infty}^{+\infty}F(z,x_z,\theta)\mathrm{d}\theta. \quad (9)$$

And the deviation distance x_m can be represented as

$$\Delta x_\mathrm{ol}=x_m=x_z-\frac{1}{2}z\theta. \quad (10)$$

Combining with Eqs. (6)(9)(10), the conditional probability is

$$\begin{aligned} H(z,x_m) &= \int_{-\infty}^{+\infty}F(z,x_z,\theta)\mathrm{d}\theta \\ &= \frac{\sqrt{3}}{2\sqrt{\pi}}\frac{w}{z^{3/2}}\exp[-3w^2x_m^2/z^3]. \end{aligned} \quad (11)$$

And the RMS deviation distance is given by

$$x_{m\,\mathrm{rms}}=\sigma_{x_m}=\left(\frac{z^3}{6w^2}\right)^{1/2}=\frac{1}{2\sqrt{3}}z\sigma_\theta=\frac{1}{2\sqrt{3}}z\theta_0. \quad (12)$$

A 100 mm long uranium object was used to simulate the blur caused by object length, the kinetic energy of proton beam is 50 GeV and the number of macro particles is 2×10^5. The distribution of deviation distance simulated by Geant4 is shown in Fig. 6 and the RMS value is 0.07 mm.

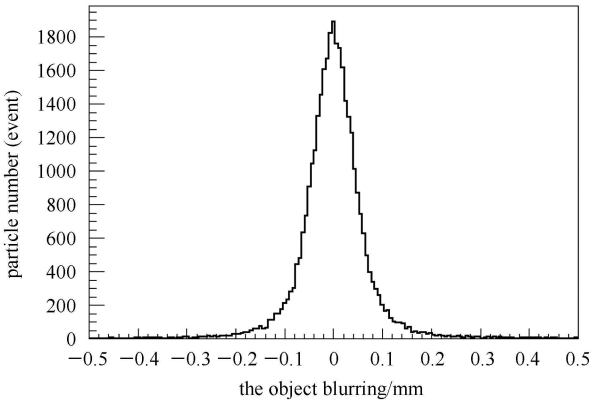

Fig. 6. The blur distribution caused by object length.

3.3 The blur caused by the back wall of the vessel

Scattering from the containment vessel which holds the object under experiment also affects the image blur and cannot be removed by the lens system [1]. The containment vessel is needed for two reasons: first, to protect the equipment from several pounds of exploding HE; and second, to confine any hazardous material used in the experiment.

As shown in Fig. 7, the incident particle passes through the front wall, the object and the back wall successively. And the scattering angles are φ_1, θ and φ_2 respectively.

In fact, the scattering between the incident particle and the front wall will not cause image blur directly, it will bring insufficient modulation of the proton beam which will be discussed in the next chapter.

The back wall of the vessel will bring image blur, and such a blur cannot be removed by using any ways and means. As can be seen in Fig. 7 the blur caused by the back wall of containment vessel is equal to the distance between Point B and Point C', i.e.,

$$\Delta x_\mathrm{ve}=-l_2\varphi_2. \quad (13)$$

The commonly used containment vessel is made of iron with 2 m radius [15], and the front wall and back wall are made of 5 cm iron or aluminum. In the case of a 50 GeV proton beam passing through such a vessel with

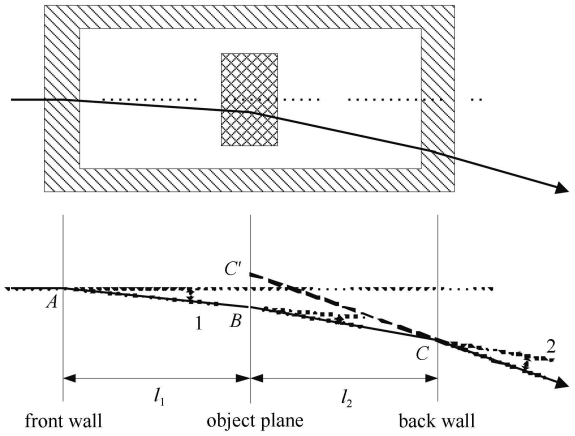

Fig. 7. Trace of an incident proton through the containment vessel in x-axis.

an iron back wall, the image blur caused by the back wall is 0.96 mm calculated by Formula (13). For an aluminum back wall, the image blur decreases to 0.4 mm.

3.4 The blur caused by beam's insufficient modulation

In actual incident beam, particles' transverse displacement x and angle deviation x' cannot be absolutely correlated because of the large beam emittance caused by space charge and scattering of the diffuser and the vessel front wall. The angle deviation can be expressed as

$$x'=\omega x+\delta x'. \tag{14}$$

As shown in Fig. 8(a) is the ideal beam distribution for pRad, but the actual one is shown in Fig. 8(b), in which α and β are the Twiss parameters, and ε is the beam emittance.

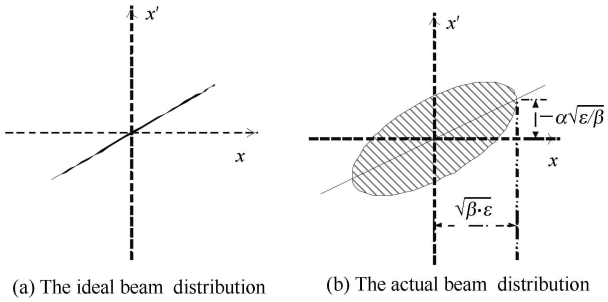

Fig. 8. The distribution of incident particles for pRad in x-axis.

As shown in Fig. 8(b), if choosing the correlation coefficient $\omega=-\alpha/\beta=-T_{116}/T_{126}$, the blur caused by the beam's insufficient modulation arrives at its minimum. In high energy pRad, the front wall of vessel has the maximal effect on emittance increase, and the scattering angle φ_1 which is caused by the front wall as shown in Fig. 7 has the biggest contribution to $\delta x'$. The image blur caused by the front wall has the same mechanism as the chromatic aberrations blur, and the expression is

$$\Delta x_{\rm im}=T_{126}\varphi_1\delta. \tag{15}$$

If the vessel front wall is made of iron, the RMS blur caused by the beam's insufficient modulation is about 0.06 mm calculated by Formula (15). And for an aluminum front wall, such a blur is about 0.025 mm.

4 Conclusion and discussion

In high energy pRad, almost all the image blurs scale inversely with the beam momentum, so a better image is therefore expected with higher beam energy.

The chromatic aberrations blur is introduced when the proton beam passes through the pRad lens system ($-$I magnetic lens typically). To decrease the chromatic aberration blur, the incident proton beam should be modulated to meet the direct proportion relation between the proton particle's transverse displacement and the angle deviation. Besides, it is also an effective solution by choosing appropriate magnetic field grads of quadrupole lens.

The maximum blur is caused by the back wall of containment vessel, as shown by Eqs. (5) and (13). It depends on the thickness of the vessel wall and the distance between the object and the vessel back wall [1]. To decrease such a blur, the determinant point is to find a lighter material with strong enough strength to meet the shock wave impact.

Compared with the back wall, the front wall of the vessel is less important, since it only affects the proton beam's modulation. In high energy pRad, the blur caused by beam's insufficient modulation can be ignored usually. But in the case of medium energy, or even low energy pRad, the un-normalized emittance is greater and the beam modulation is worse, such a blur must be considered carefully.

The blur caused by object length is introduced as the protons are scattered and their transverse displacements in the object plane are changed. Commonly, the experimental object is determined, and the only improved approach is to increase the beam energy.

References

1 Ziock H J, Adams K J, Alrick K R et al. The Proton Radiography Concept, LA-UR-98-1368. Available: http://lib-www.lanl.gov/la-pubs/00460235.pdf

2 Morris C L. Proton Radiography for an Advanced Hydrotest Facility, LA-UR-00-5716. Available: http://lib-www.lanl.gov/la-pubs/00357005.pdf

3 WEI Tao, YANG Guo-Jun, HE Xiao-Zhong et al. Chinese Physics C (HEP & NP), 2010, **34**(11): 1754–1756

4 DENG Jian-Jun, CHENG Lian-An, WANG Hua-Chen et al. Linear Induction Electron Accelerator. Beijing: National Defence Industry Press, 2006. 1–12 (in Chinese)

5 Hogan G E, Adams K J, Alrick K R et al. Proton Radiography. Proceedings of the 1999 Particle Accelerator Conference. New York

6 Koehler A M. Proton Radiography. Science, 1968, **160**(3825): 303–304

7 Frank Merrill. Proton Radiography Primer, LA-UR-08-07298

8 Christopher Morris, Hopson J W, Philip Goldstone. Proton Radiography. Los Alamos Science, 2006, **30**: 32–44

9 WEI Tao, YANG Guo-Jun, LONG Ji-Dong et al. Chinese Physics C (HEP & NP), 2012, **36**(7): 1–5

10 SHI Jiang-Jun. High Energy Radiography Theory. Graduated Schoolbook for Chinese Academy of Engineering Physics, 2007. 231–232 (in Chinese)

11 Mottershead C T, Zumbro J D. Magnetic Optics for Proton Radiography. Proceedings of the 1997 Particle Accelerator Conference. Vancouver, B. C., Canada

12 HE Xiao-Zhong, YANG Guo-Jun, LIU Chen-Jun. High Power Laser and Particle Beams, 2008, **20**(2): 297–300 (in Chinese)

13 XIE Yi-Gang et al. Particle Detectors and Data Acquisition. Beijing: Science Press, 2003. 10–12 (in Chinese)

14 Agostinelli S et al. NIMA, 2003, **506**: 250–303. Available: http://geant4.web.cern.ch/geant4/

15 LIU Jin, ZHANG Lin-Wen, LIU Jun et al. High Power Laser and Particle Beams, 2008, **20**(7): 1199–1202 (in Chinese)